Three-dimensional structure of the thermal boundary layer in turbulent Rayleigh-Bénard convection: A Lagrangian perspective

György Tegze* and Frigyes Podmaniczky
HUN-REN Wigner Research Centre for Physics, H-1525 Budapest, Post Office Box 49, Hungary

(Received 7 September 2023; accepted 3 May 2024; published 8 July 2024)

In turbulent Rayleigh-Bénard convection, it is generally acknowledged that the thermal boundary layer (BL) governs heat transfer, although its scaling with the Rayleigh number is still debated. Various methods have been developed to measure the characteristic thickness of the BL, which are mostly employed in a time-averaged manner. Among them, only the slope method can be applied in an instant of time, being therefore capable of time-resolved analysis; however, it provides no further insight when the Nusselt number is known. Accordingly, the average properties of the BL are thoroughly studied, mainly in the context of heat transfer; its time-dependent structural dynamics and roughness remain largely unexplored. Here, we propose a Lagrangian method to characterize both the time-averaged and the spatio-temporal evolution of the BL, that marks the edge of the BL where convective and diffusive transports overlap. The characteristic thickness of the BL, that is defined by this method, is not a trivial function of the Nusselt number and can be considered a potential tool to analyze the BL structure while varying the Nusselt number. It is also demonstrated using 3D direct numerical simulations, that the injection of heat is extremely inhomogeneous in space and time; the vast majority of heat accumulates in narrow domains, that is governed by the local plume dynamics.

DOI: 10.1103/PhysRevFluids.9.074602

Buoyancy-driven flows are common in nature surrounding us, including thermal convection in the atmosphere [1], in the oceans [2], or inside buildings [3]. Also, it is generally acknowledged that such phenomenon occurs in geophysical [4] and astrophysical [5] flows, such as in the earth's mantle, or inside the sun. Additionally, numerous technological processes, such as liquid metal processing [6] requires the understanding of buoyancy-driven flows. In these real-world phenomena, buoyancy is often accompanied by geometrical complexity, additional forces (e.g., inertial or magnetic) or multiple origins of change in density. To gain fundamental understanding either theoretically or experimentally, it is often useful to rely on a simplified model, that lacks additional complexity, but still addresses major aspects of the observations. Rayleigh-Bénard convection (RBC) is a fluid dynamical setup, in which a fluid layer is subjected to thermal expansion: it is heated at the flat bottom plate, and cooled at the top plate. Despite its apparent simplicity, it is one of the classical problems in fluid dynamics; however, the scaling ($\mathrm{Nu} \propto \mathrm{Ra}^{\gamma}\mathrm{Pr}^{\chi}$) with fluid properties (Ra, Pr) of heat transfer (Nu) through an RBC cell is still debated. Here, the Nusselt number (Nu) is expressed in terms of other dimensionless parameters: Ra the Rayleigh number and Pr the Prandtl number.

It is generally agreed that the heat flux through the RBC cell is limited by heat diffusion through thermal boundary layers (BL) near the top and bottom plates characterized by vanishing convective heat transfer. Indeed, most theories, that predict the scaling laws for Nu are essentially BL theories:

*tegze.gyorgy@wigner.hu

including mixing layer theories [7,8], various turbulent BL theories [9–12], and their variants [13]. These theories are based on distinct fundamental assumptions on the kinetic and the thermal BL and occasionally result in different scaling exponents in various regimes of Ra and Pr [14]. Moreover, Grossmann and Lohse have identified regimes for the scaling law and plotted a kinetic phase diagram based on the significance of kinetic and thermal energy dissipation in the BL versus in the bulk, and the relative magnitude of kinetic and thermal BL widths (λ_u and λ_θ) [12]. Therefore, in the case of RBC, it is of great importance to both qualitatively and quantitatively characterize the BL properties to validate or challenge the underlying hypotheses of the various BL theories.

Due to the no-slip boundary conditions, the heat transfer is purely diffusive at the heated/cooled plates, which changes character through the boundary layer and becomes dominated by convection in the bulk. Conceptually, the BL is understood in a time-averaged fashion, and it is assumed to be spatially contiguous, which may vary in thickness (λ_θ). Indeed, traditionally λ_θ is defined through average properties of the temperature time-series measured at different distances from the top/bottom plates. The classical 99% threshold method explicitly relies on measuring the time-averaged temperature ($\lambda_\theta^{99\%}$), while Belmonte *et al.* [15] have used the root-mean-squared (RMS) temperature fluctuations ($\lambda_\theta^{\mathrm{rms}}$) to define the boundary layer width. These methods necessitate averaging times, which exceed the timescale of the slowly evolving large-scale convection (LSC) patterns. The third, and most common is the slope method ($\lambda_\theta^{\mathrm{sl}}$), in which the temperature profiles near the plates are fitted with a linear function of the coordinate, which gives a spatial extent by a simple geometrical construction [14]. $\lambda_\theta^{\mathrm{sl}}$ is related to the Nusselt number at the boundary by a simple inverse relation $\lambda_\theta^{\mathrm{sl}} \propto 1/\mathrm{Nu}$. Accordingly, it holds no further information as long as the Nusselt number is known. The construction is based on the assumption, that the heat transfer is purely diffusive inside the boundary layer and is separated sharply from the purely convective bulk domain, therefore it does not account for the inherently smooth transition between distinct regions of heat transfer. However, the spatial roughness of the boundary layer can be examined, since it does not necessarily require either temporal or spatial averaging. Nevertheless, it was successfully used by Schumacher and Pandey [16,17] to characterize the instantaneous and/or local properties of the BL and they have concluded that $\lambda_\theta^{\mathrm{sl}}$ is smaller where plumes are impacting the plates and larger in regions where plumes are leaving the plates. The above methods commonly use Eulerian sampling for measuring the temperature at fixed locations; however, Lagrangian experiments, which sample along fluid pathlines, are also available [18].

Herein, we present a method to define the BL width that allows the structural analysis with high spatial and temporal resolution. The temporal change of the temperature ($\partial_t T$) is computed along Lagrangian trajectories of passive tracers, thus removing the convective component and characterizing the purely diffusive heat transport. $\partial_t T$ curves show distinct extrema near the boundaries when plotted against either the vertical position of the tracers or time. The distances of the extrema from the top/bottom plates define a characteristic length for the thermal BL, which we propose to use both for spatially resolved and averaged analysis of the BL. The length defined this way is not a trivial function of the Nusselt number, therefore holds additional information about the boundary layer. Also, contrary to the construction of $\lambda_\theta^{\mathrm{sl}}$, it accounts for the smooth transition between the diffusive and convective regimes.

The thermal convection in the RBC is described by momentum, energy, and mass balance equations, which in the Oberbeck-Boussinesq approximation [19,20] and in natural nondimensional units, can be written as follows:

$$\frac{\partial \mathbf{u}}{\partial t} + \mathbf{u}\cdot\nabla\mathbf{u} = -\nabla p + \theta\mathbf{e_z} + \sqrt{\frac{\mathrm{Pr}}{\mathrm{Ra}}}\nabla^2\mathbf{u}, \tag{1}$$

$$\frac{\partial \theta}{\partial t} + \mathbf{u}\cdot\nabla\theta = \frac{1}{\sqrt{\mathrm{PrRa}}}\nabla^2\theta, \tag{2}$$

$$\nabla\cdot\mathbf{u} = 0. \tag{3}$$

The dimensionless numbers Ra and Pr come from scaling the length with the box height (H) and the velocity with the free-fall velocity (v_{ff}), the velocity of a fluid parcel, which corresponds to the kinetic energy when converted from the maximum of the buoyant potential energy. While $\theta = (T - T_{\mathrm{cold}})/(T_{\mathrm{hot}} - T_{\mathrm{cold}})$ is the temperature scaled by the temperature difference between the plates.

For the numerical solution of the governing equations the finite volume method is applied. Spatial and temporal discretization of the equations was done using the central differencing scheme (CDS) and forward Euler time integration, respectively. We note, that the above forward time central space (FTCS) discretization in the convection dominated regime is very restrictive for the applicable stable time-step [21] but in turn offers low numerical diffusion. The momentum Eq. (1) is coupled to the incompressibility constraint Eq. (3) using Chorin's projection method [22], whereas Goda's incremental pressure correction method [23] was chosen in the projection step to improve the convergence characteristics of the algebraic solver via providing improved initial guess for the velocities. A custom multigrid method, which is optimized for modern massively parallel hardware (GPU) was used to solve the algebraic equations in the correction step [24]. The simulation was performed at $\mathrm{Ra} = 10^7$, $\mathrm{Pr} = 0.7$ and aspect ratio $\Gamma = 0.5$ on a $400\times400\times800$ numerical grid and using $\Delta t = 1.64\times10^{-4}$ timestep in free-fall time units. The above setup allows a well-resolved analysis of the BL, which is confirmed by convergence analysis of the time-averaged properties with increasing numerical resolution. Velocity and temperature fields were sampled along Lagrangian trajectories using tri-linear interpolation, while tracer pathlines were computed by explicit time-integration. The compute code was implemented and executed on a multi-GPU workstation.

In the simulation spanning 300 free-fall time units, we have placed 10^6 randomly distributed passive tracers into the simulation domain, and their trajectories were used to sample the fluid properties (Θ, $\partial_t\Theta$, and $\mathbf{u}$) along their trajectories. Sampling was started at 150 free-fall time to ensure statistical steady state, and high sampling resolution was chosen (0.0375 free-fall time unit) to resolve the spatio-temporal details of the boundary layer. We denote symbols for quantities obtained by Lagrangian sampling, with uppercase (e.g., Θ). We note here that $\partial_t\Theta$ is the temperature-change due to pure diffusion, since it represents the substantial derivative as it is computed along the tracer trajectory. Accordingly, instantaneous features of the $\partial_t\Theta$ can be computed from Eulerian temperature and velocity data by directly computing the substantial derivative. First, we examine spatio-temporal $\langle\cdot\rangle_{\mathrm{st}}$ and $\langle\cdot\rangle_{\mathrm{s}}$ spatial (binned) averages of these quantities as the distance is increased from the bottom hot plate Fig. 1(a). The $\langle\Theta\rangle_{\mathrm{st}}$ across the boundary layer shown are identical to data obtained from Eulerian measurements using random sampling positions. Generally, the mean BL width $\lambda_\Theta^{\mathrm{sl}}$ and the corresponding Nu is derived using the $\langle\Theta\rangle_{\mathrm{st}}$ profile. However, snapshots of the spatially averaged $\langle\Theta\rangle_{\mathrm{s}}$ profiles show notable variation in time and space indicating that the thermal BL is not homogeneous in space and time. It is known from previous studies, that the BL width derived from time-averaged data show spatial variation, thinner at the center and wider close to the walls [25]. In a recent analysis of 2D DNS [17] it was found, that the local BL is thinner in spatial regions of plume impact compared to regions of plume ejection. To analyze the effect of plume dynamics on the BL, tracers are split by the sign of u_z; positive values belong to emerging hot, while negative values belong to impacting cold plumes. The profile of $\langle\Theta\rangle_{\mathrm{s}}$ shows pronounced differences Fig. 1(b) and indicates that the flow structure has significant impact on heat transfer.

We followed the same procedure with $\partial_t\Theta$, which is computed along tracer trajectories as a Lagrangian quantity. Plotting $\langle\partial_t\Theta\rangle_{\mathrm{st}}$ and $\langle\partial_t\Theta\rangle_{\mathrm{s}}$ versus the distance from the bottom plate Fig. 1(c) shows a very distinct maximum similar to the RMS profile of Θ fluctuations [15]. The maximum near the bottom plate and the minimum next to the top plate define the Lagrangian width of the thermal BL $\langle\lambda_\Theta^{\mathrm{Lag}}\rangle_{\mathrm{st}}$. For our RB setup, the computation of the BL width using the conventional slope method and our proposed Lagrangian method gives significantly different values; $\langle\lambda_\Theta^{\mathrm{sl}}\rangle_{\mathrm{st}} = 0.0313$ and $\langle\lambda_\Theta^{\mathrm{Lag}}\rangle_{\mathrm{st}} = 0.0181$, respectively. However, systematic study is needed to compare the scaling behavior with the parameters Ra and Pr, which is of prime interest. The value $\langle\lambda_\Theta^{\mathrm{Lag}}\rangle_{\mathrm{st}}$ separates domains of different thermal behavior; I. in the vicinity of the plates, quasi-steady diffusive behavior

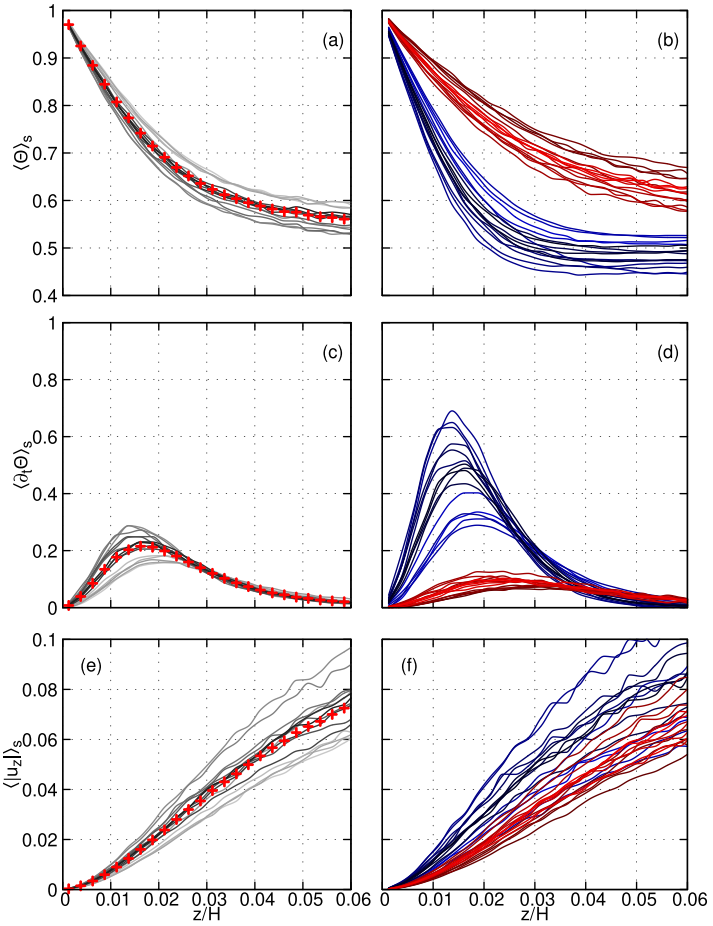

FIG. 1. Spatial averages of (a) Θ, (c) $\partial_t\Theta$, and (e) $|u_z|$ at random time instances are shown with solid lines, the values are computed with H/400 bin-resolution on the vertical position of the tracers. Spatio-temporal averages $\langle\cdot\rangle_{\rm st}$ are plotted with $+$ marks. The horizontal spacing of the data points corresponds to double grid spacing. Panels (b), (d), (e) show the same quantities, but tracers in emerging plumes (red) and impacting plumes (blue) are distinguished by the sign of u_z and the spatial averages were computed selectively.

(on short timescales) is characterized by a linear Θ profile. II. the bulk domain, where coherent convection or mixing takes place and results in low absolute values of $\langle\partial_t\Theta\rangle_s$. In between, there is a subtle interaction of the two domains that results in the accumulation of thermal and kinetic energy. At $\langle\lambda_\Theta^{\rm Lag}\rangle_{\rm st}$, the rate of energy injection is maximal. Integrating the $\langle\partial_t\Theta\rangle_{\rm st}$ profile near the plates Fig. 1(b) gives the convective heat current throughout the bulk domain. The diffusive current in the bulk is defined by the slope of $\langle\Theta\rangle_{\rm st}$ in the bulk. Computing these quantities provides an alternative route to define Nu that is consistent with the Lagrangian definition of the BL width. It is also worth mentioning that the vertical velocity magnitude $|u_z|$ is nonnegligible throughout the thermal BL Fig. 1(e).

The Lagrangian definition of λ_Θ does not explicitly require time averaging, therefore it allows the separation of tracers for inbound and outbound plumes at a single instance of time. Separating sample trajectories by the sign of u_z provides evidence that the accumulation of energy is spatially inhomogeneous; the vast majority concentrates near impacting plumes Fig. 1(d). However, we note that spatial averaging hides the structure of the BL.

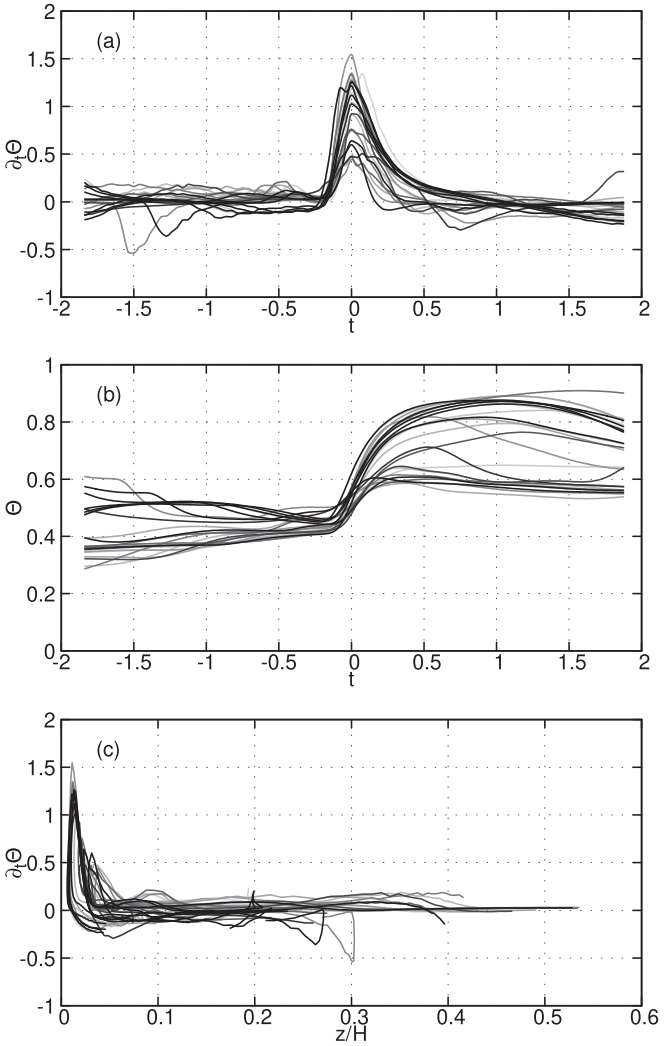

FIG. 2. Samples of thermal quantities in fluid parcels which enter the thermal boundary layer at an instance of time (translated to $t = 0$): (a) the rate of change of temperature $\partial_t\Theta$ and (b) the temperature Θ vs time are plotted along the pathlines. Panel (c) shows $\partial_t\Theta$ vs the vertical positions, here the location of maxima corresponds to the local boundary layer width.

Finer details are uncovered when those trajectories are sampled which pass through the BL at a given time. Previous results for the spatially averaged profiles foreshadow that $\partial_t\Theta$ along the pathlines may show characteristic extrema with respect to time. Those set of trajectories are selected that show extrema in $\partial_t\Theta$ at a time instance (fixed at $t = 0$), see Fig. 2(a), the location of these extrema can be considered as the edge of the boundary layer. The vertical extent of the boundary layer can be read off when $\partial_t\Theta$ is plotted against the z coordinate for the selected trajectories, see Fig. 2(c).

Before reaching the boundary layer (approximately $t < -0.25$) pathlines trace back deeply into the bulk of the domain, as shown in Figs. 2(c) and 3. This provides evidence that no well-mixed layer exists between the BL and the bulk domain as assumed by Castaing *et al.* [8], the diffusion dominated BL interacts directly with the impacting plumes, at least under the conditions the analysis

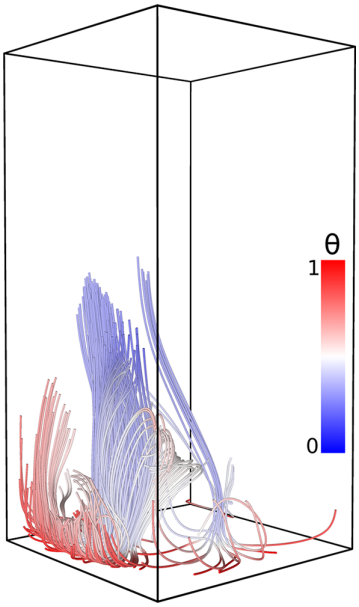

FIG. 3. Pathlines of trajectories passing through the boundary layer edge at the same instance of time colored by temperature (Θ).

was performed. $\partial_t \Theta$ either fluctuates (approximately around zero) in the regions of heavy turbulent mixing, or it is close to zero when the trajectory samples a coherent turbulent structure.

After passing the maximum of $\partial_t \Theta$ ($t > 0$) the temperature (Θ) further increases and reaches a maximum, see Fig. 2(b) and accordingly $\partial_t \Theta$ changes sign as the pathline returns to the bulk domain. This unique BL analysis method makes it apparent, that a characteristic time is present in the boundary layer dynamics, which coincides with the time interval that the trajectory spends in the boundary layer. This characteristic time can alternatively be defined by the half-width of the peaks in $\partial_t \Theta$ as displayed in Fig. 2(a), which relates to a smooth transition from the bulk to the boundary layer. We also note, that the computation of the characteristic time requires the explicit tracking of the fluid parcels, thus it cannot be derived from instantaneous snapshots of Eulerian data.

Finally, the three dimensional morphology of maximum energy injection is presented at an instance of time. These points can be considered as markers of the boundary layer edge in the regions of inbound convection. Results in the previous sections based on spatially averaged data suggest, that heat transfer is highly inhomogeneous and localized to impacting plumes. It is also confirmed by trajectory analysis: plotting the spatial positions identified as the BL edge provides evidence that the BL is not just inhomogeneous but also the injection of the thermal energy is noncontiguous on the BL edge. The intersections of the tracer trajectories with the BL edge is plotted in Figs. 4(a) and 4(b). The boundary layer width (shown as color code) is thinner at the center of the plume and thicker at the edge of the plume. This behavior is in line with previous observations of the time averaged BL [25].

Our proposed method separates diffusive change in thermal energy from convective effects, thus signaling the injection of potential energy due to change in density at the edge of the thermal boundary layer. Analyzing single time instances, it was found, that regions in which incoming plumes impact, contribute the vast majority of the potential energy excitation in the RBC system. Accordingly, the contribution of emerging plumes is negligible; the thermal excitation at the edge of the BL can be considered to be spatially noncontiguous. It is remarkable that the proposed analysis method of the thermal boundary layer is not restricted to simple geometries; thus, it can be applied for rough or uneven surfaces and complex domains.

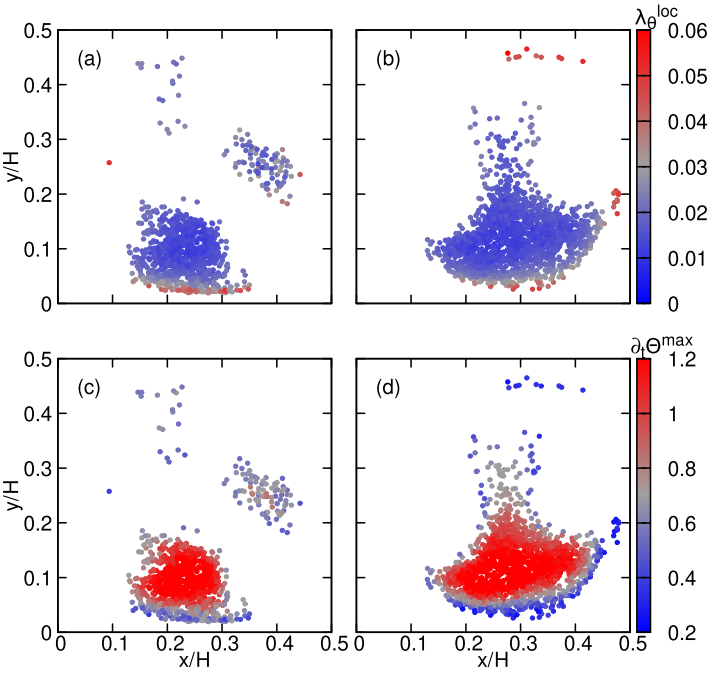

FIG. 4. The spatial arrangement of the Lagrangian boundary layer is shown, sampled at two instances of time (left and right columns). The lateral x-y plane of the simulation box forms the axes of the subplots, while the distance of the sample points from the bottom plate are color coded in the first row, in panels (a) and (b), up to the boundary layer width λ_Θ^{loc}. The time evolution of λ_Θ^{loc} is also available as supplemental animation file [26]. Panels (c) and (d) show the maximum values of the injected thermal energy ($\partial_t\Theta^{max}$) at the boundary layer edge for the same samples as in the first row. See the time evolution of λ_Θ^{loc} on supplemental animation file [26].

This work was supported by the National Research, Development and Innovation Office (NKFIH), Hungary under Contract No. KKP-126749.

[1] O. M. Pauluis and J. Schumacher, Self-aggregation of clouds in conditionally unstable moist convection, Proc. Natl. Acad. Sci. USA **108**, 12623 (2011).
[2] R. W. Schmitt, Double diffusion in oceanography, Annu. Rev. Fluid Mech. **26**, 255 (1994).
[3] G. Hunt and P. Linden, The fluid mechanics of natural ventilation–displacement ventilation by buoyancy-driven flows assisted by wind, Build. Sci. **34**, 707 (1999).
[4] B. A. Buffett and C. T. Seagle, Stratification of the top of the core due to chemical interactions with the mantle, J. Geophys. Res.: Solid Earth **115**, B04407 (2010).
[5] C. Paladini, F. Baron, A. Jorissen, J.-B. Le Bouquin, B. Freytag, S. Eck, M. Wittkowski, J. Hron, A. Chiavassa, J. Berger, C. Siopis, A. Mayer, G. Sadowski, K. Kravchenko, S. Shetye, F. Kerschbaum, J. Kluska, and S. Ramstedt, Large granulation cells on the surface of the giant star π^1 gruis, Nature (London) **553**, 310 (2018).
[6] P. Kumar, K. Srinivasan, and P. Dutta, Visualization of convection loops due to Rayleigh–Benard convection during solidification, Mech. Res. Commun. **33**, 593 (2006).
[7] R. H. Kraichnan, Turbulent thermal convection at arbitrary Prandtl number, Phys. Fluids **5**, 1374 (1962).

[8] B. Castaing, G. Gunaratne, F. Heslot, L. Kadanoff, A. Libchaber, S. Thomae, X.-Z. Wu, S. Zaleski, and G. Zanetti, Scaling of hard thermal turbulence in Rayleigh-Bénard convection, J. Fluid Mech. **204**, 1 (1989).
[9] B. I. Shraiman and E. D. Siggia, Heat transport in high-Rayleigh-number convection, Phys. Rev. A **42**, 3650 (1990).
[10] B. Dubrulle, Scaling in large Prandtl number turbulent thermal convection, Eur. Phys. J. B **28**, 361 (2002).
[11] M. Hölling and H. Herwig, Asymptotic analysis of heat transfer in turbulent Rayleigh–Bénard convection, Int. J. Heat Mass Transf. **49**, 1129 (2006).
[12] S. Grossmann and D. Lohse, Scaling in thermal convection: A unifying theory, J. Fluid Mech. **407**, 27 (2000).
[13] E. Lindborg, Scaling in Rayleigh–Bénard convection, J. Fluid Mech. **956**, A34 (2023).
[14] G. Ahlers, S. Grossmann, and D. Lohse, Heat transfer and large scale dynamics in turbulent Rayleigh-Bénard convection, Rev. Mod. Phys. **81**, 503 (2009).
[15] A. Belmonte, A. Tilgner, and A. Libchaber, Temperature and velocity boundary layers in turbulent convection, Phys. Rev. E **50**, 269 (1994).
[16] J. Schumacher, V. Bandaru, A. Pandey, and J. D. Scheel, Transitional boundary layers in low-Prandtl-number convection, Phys. Rev. Fluids **1**, 084402 (2016).
[17] A. Pandey, Thermal boundary layer structure in low-Prandtl-number turbulent convection, J. Fluid Mech. **910**, A13 (2021).
[18] Y. Gasteuil, W. L. Shew, M. Gibert, F. Chillá, B. Castaing, and J.-F. Pinton, Lagrangian temperature, velocity, and local heat flux measurement in Rayleigh-Bénard convection, Phys. Rev. Lett. **99**, 234302 (2007).
[19] A. Oberbeck, Ueber die wärmeleitung der flüssigkeiten bei berücksichtigung der strömungen infolge von temperaturdifferenzen, Ann. Phys. **243**, 271 (1879).
[20] J. Boussinesq, Théorie analytique de la Chaleur mise en harmonie avec la thermodynamique et avec la théorie mécanique de la lumière, Monatsh. f. Mathematik und Physik **15**, A67 (1904).
[21] A. C. Hindmarsh, P. M. Gresho, and D. F. Griffiths, The stability of explicit euler time-integration for certain finite difference approximations of the multidimensional advection–diffusion equation, Int. J. Numer. Methods Fluids **4**, 853 (1984).
[22] A. J. Chorin, Numerical solution of the Navier-Stokes equations, Math. Comput. **22**, 745 (1968).
[23] K. Goda, A multistep technique with implicit difference schemes for calculating two- or three-dimensional cavity flow, J. Comput. Phys. **30**, 76 (1979).
[24] G. Tegze and G. I. Tóth, A GPU cluster optimized multigrid scheme for computing unsteady incompressible fluid flow, arXiv:1309.7128.
[25] S.-L. Lui and K.-Q. Xia, Spatial structure of the thermal boundary layer in turbulent convection, Phys. Rev. E **57**, 5494 (1998).
[26] See Supplemental Material at http://link.aps.org/supplemental/10.1103/PhysRevFluids.9.074602 for the animations [lambda.avi] and [dtdttheta.avi].